Rapid Communications

Mass transport through dislocation network in solid ^{4}He

Jaeho Shin and Moses H. W. Chan*

Department of Physics, The Pennsylvania State University, University Park, Pennsylvania 16802-6300, USA

(Received 24 September 2018; published 8 April 2019)

We studied the transport of ^{4}He atoms through 2.5-mm-thick solid ^{4}He samples sandwiched between two superfluid leads with five different tailor-made sample cells. Measurements in a cell with a barrier at the center of the solid samples and in a cell filled with silica aerogel establish the causal relation between the observed mass flow and the dislocation network in the solid sample. Comparing the results from these cells and prior measurements on solid samples with thicknesses of 2 cm and 8 μm reveals that the mass flow rate decreases logarithmically with the thickness of the solid ^{4}He. Interestingly, the mass flow exhibits both superfluid and bosonic Luttinger liquid characteristics at low temperature.

DOI: 10.1103/PhysRevB.99.140502

Superfluidlike mass flow through 2-cm-thick solid ^{4}He samples sandwiched between superfluid leads was first observed at the University of Massachusetts (UMass) [1–5]. This phenomenon was replicated recently at Penn State through solid samples of only 8 μm thickness [6]. Mass flow through the superfluid-solid-superfluid sandwich can be initiated by direct injection of ^{4}He to one end of the sandwich or by imposing a superfluid fountain pressure across the sandwich. Quantum Monte Carlo simulation studies proposed that the dislocation network in solid ^{4}He is responsible for the mass flow phenomenon. The simulations found both the screw and edge dislocations with a Burgers vector along the c axis of hcp solid ^{4}He have superfluid cores that can support the transport of ^{4}He atoms along the dislocation lines [7,8]. In addition, a superclimb process that adds or eliminates basal planes at edge dislocations with a superfluid core was proposed for creating a density gradient in the solid sample in response to the chemical potential that drives the flow [8,9]. However, a direct causal connection between the mass flow and dislocation network has yet to be established in experiments. Indeed, direct compression of the solid shows evidence of mass flow without any superfluid leads [10] and the flow was interpreted to take place along a surface superfluid layer between the sample cell wall and the solid sample rather than through the solid.

In this Rapid Communication, we report measurements on solid ^{4}He samples confined in five tailor-made sample cells (Fig. 1) to confirm directly the causal relation between mass flow and the dislocation network and also to understand the exact mechanism of the transport of ^{4}He atoms through the dislocation network. All five sample cells are geometrically similar to the 8-μm cell of Ref. [6]. The results from the cell C-R are used as references for other sample cells. Sample cell C-B has a barrier in the form of a thin copper foil suspended in the center of the cell that can effectively block mass flow through the solid. Sample cell C-A is completely filled with silica aerogel of 95% porosity. The silica strands in the aerogel are randomly interconnected with a mean separation of 100 nm [11,12], orders of magnitude shorter than the typical loop length of a dislocation network of 10 μm [13,14]. As a consequence, a dislocation network cannot form in this cell. The results from sample cells C-B and C-A conclusively show that the dislocation network embedded in solid ^{4}He is responsible for the mass flow. Sample cells C-$G\perp$ and C-$G\parallel$ are installed with highly oriented pyrolytic graphite (HOPG) with the c axis aligned respectively perpendicular and parallel to the flow direction to seed hcp single crystals of ^{4}He with the same alignment [15]. Since the basal planes of a solid ^{4}He crystal are perpendicular to the flow path in the C-$G\parallel$ cell, the superclimbing of the edge dislocation will be strongly suppressed. On the other hand, the crystal orientations of the C-$G\perp$ cell are ideal for superclimbing. (Details on the installation and cleaning of graphite are described in the Supplemental Material Sec. I [16].) While confirming that the mass flow does take place along the dislocation lines, the results from C-$G\parallel$, C-$G\perp$, and C-R show no evidence that the superclimb process played an important role in determining the mass flow rate.

Two porous glass rods that serve as superfluid leads are inserted into the opposite ends of each of the five copper sample cells. The exact dimensions of the five solid ^{4}He samples are given in the caption of Fig. 1. The sample cells are strongly thermally attached to the mixing chamber of the dilution refrigerator. The high-temperature ends of the porous glass rods open to small bulk liquid reservoirs SL and SR and are then connected via thin capillaries to the ^{4}He gas manifold at room temperature. The pressures of the capillaries are read with piezoelectric pressure gauges PL and PR (see Fig. 1). Porous Vycor glass rods of 4.6 mm in diameter and 40 mm in length are used for sample cells C-R, C-B, C-A, C-$G\perp$, and also the 8-μm cell of Ref. [6]. Porous glass rods AGC40 [17] with a diameter of 3.5 mm and also 40 mm length are used for C-$G\parallel$. AGC40 has the same microstructure as Vycor glass, except the internal pores have a diameter of $\sim$4 nm instead of 7 nm. The temperature of reservoirs SL and SR, read by thermometers TL and TR, are controlled by

*Corresponding author: MHC2@psu.edu

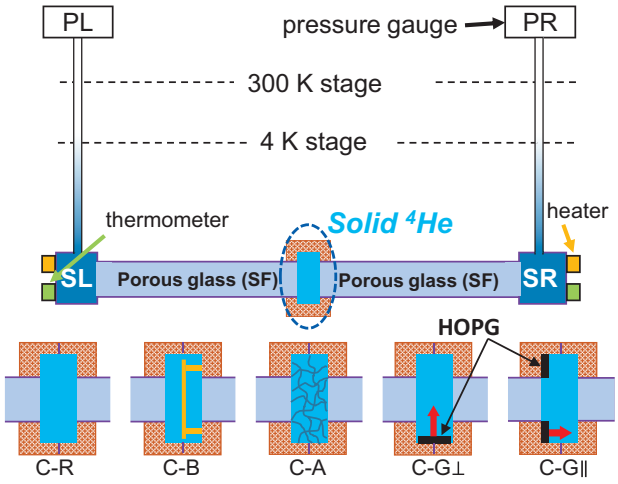

FIG. 1. Schematic drawing showing the configuration of the superfluid-solid-superfluid sandwich and the five different sample cells. *C-R* has a cylindrical disk-shaped sample space for solid ^{4}He. *C-B* has a barrier in the form of a thin copper foil suspended with three pins in the center of the sample space. The cross-sectional area of the barrier is 126.6 mm^2, which is 92% of that of the solid sample and 760% that of the porous glass rod. *C-A* is completely filled with silica aerogel of 95% porosity. HOPG crystals are glued in *C-G*⊥ and *C-G*∥ to the aligned *c* axis of the ^{4}He crystal to be respectively perpendicular and parallel to the flow direction. Red arrows indicate the *c* axis of the HOPG crystals. The thicknesses of the sample space are 2.5, 1.9, and 2.4 mm, and the diameters of the sample space are 13.3, 8, and 11 mm for the *C-R*, *C-G*⊥, and *C-G*∥, respectively. The thicknesses and diameters of the sample spaces in *C-B* and *C-A* are identical to that of *C-R*.

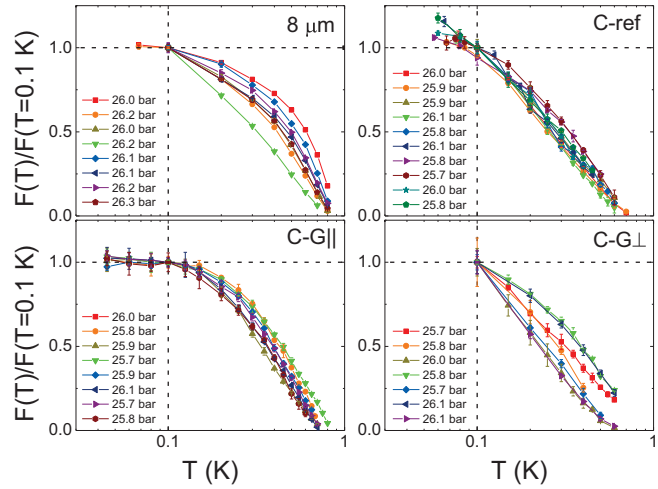

FIG. 2. Normalized temperature dependence of mass flow rates of low-pressure solid samples grown in different cells. Results from the 8-μm cell are also shown for comparison. The mass flow rate is normalized by the flow rate at 0.1 K. The flow rate increases with decreasing temperature and is sample dependent. The flow rate of solid samples in *C-G*∥ begins to saturate below 0.2 K and becomes independent of temperature below 0.1 K. This saturation is not seen in solid samples grown in *C-R* and *C-G*⊥.

heaters on the reservoirs to compensate for the heat drained (via thin copper wires) to the still of the dilution refrigerator. If the bulk liquid helium in the reservoirs is in the superfluid phase, the heaters can be and are used to create a fountain pressure across the sandwich to induce mass flow through the solid samples. We use ^{4}He gas with 0.3-ppm ^{3}He to grow solid samples. The solid samples are grown at 0.5 K from the superfluid by adding ^{4}He from a room-temperature manifold to the sample cell while maintaining a "flow field," i.e., with ^{4}He flowing from one capillary to the other through a superfluid-solid-superfluid sandwich. After a solid sample showing mass flow is grown, it can be densified (de-densified) by gradually increasing (decreasing) the pressure.

Figure 2 shows normalized mass flow as a function of temperature for low-pressure (25.7–26.3 bars) solid ^{4}He samples grown in *C-R*, *C-G*⊥, and *C-G*∥. Flow rates are normalized by the flow rate at 0.1 K. Results on similar low-pressure samples from the 8-μm cell are also shown for comparison. The as-measured, prior to normalization, flow rates are shown in Supplemental Material Sec. II [16]. Mass flow is found in all the samples and the flow rates shown are reproducible upon warming and cooling between 40 mK and 0.8 K. The flow rate of all samples from *C-G*∥ begins to saturate below 0.2 K and flattens out below 0.1 K. This saturation is not seen in other cells. The difference may be related to the fact that the *c* axes of the crystalline ^{4}He solid samples in *C-G*∥ are aligned with the flow direction. The magnitudes of the flow rate found in all sample cells shown in Fig. S2 in the Supplemental Material are sample dependent. The measured flow rates at 0.1 K of the samples in *C-R*, *C-G*⊥, and *C-G*∥, normalized by the cross-sectional area of the porous glass rod, are comparable and cluster between 5 and 25 ng/s mm^2. In comparison, the 0.1-K flow rate of the low-pressure solid samples in the 8-μm cell ranges between 35 and 70 ng/s mm^2 with one low value at 10 ng/s mm^2.

We have made measurements of the mass flow of higher-pressure samples with *C-R*. The onset temperature of mass flow decreases with increasing pressure, similar to that found in the 8-μm cell [6]. The phase boundary separating regions with and without mass flow is shifted to a lower temperature as compared to the 8-μm-thick samples. More details are shown in Supplemental Material Sec. III [16].

We have also made flow rate measurements on a series samples densified from the same "seed" sample grown from a superfluid. As noted above, a solid sample with mass flow can be densified or de-densified by changing the sample pressure. While the flow rate of each new "seed" solid sample is sample dependent, the flow rate of the 8-μm samples densified and subsequently de-densified from the same seed decays exponentially with the pressure of the sample and the rate is reproducible upon pressurization and depressurization [6]. Identical behavior is found in 2.5-mm-thick similarly densified and de-densified samples in *C-R* and *C-G*∥ cells. The exponential pressure dependence, as we have pointed out in Ref. [6], is not consistent with the model [18,19] that the observed mass flow is the consequence of liquid channels in the solid. The pressure-dependent results are shown in Supplemental Material Sec. IV [16].

In Fig. 3, we show the flow rate at 0.1 K of the four cells shown in Fig. S2 together with those grown in *C-B*

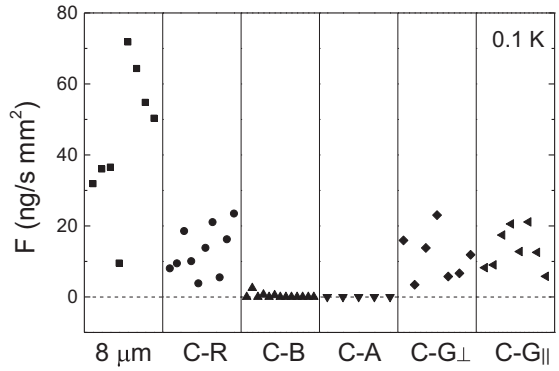

FIG. 3. Mass flow rate at 0.1 K of low-pressure solid samples in 8-μm, *C-R*, *C-B*, *C-A*, *C-G*⊥, and *C-G*∥ cells. The barrier in *C-B* is very effective in blocking mass flow through the solid samples. All solid samples grown in aerogel show no mass flow below 0.8 K.

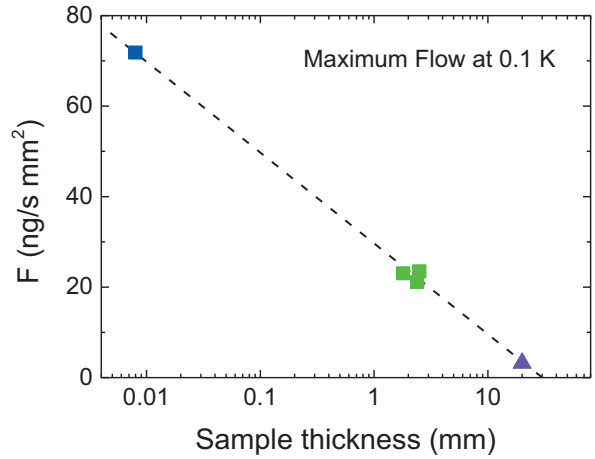

FIG. 4. The maximum mass flow rate found among all the solid samples measured in each of the five sample cells as a function of sample thickness at 0.1 K. The purple triangle is estimated from Ref. [5]. The plot shows the flow rate decreases logarithmically with sample thickness.

and *C-A*. Eight out of the 11 solid samples grown in *C-B* show no measurable mass flow and the other three show rates of just 2.52, 0.69, and 0.49 ng/s mm^2. The absence of any measurable flow in most samples and a tenfold reduction in others demonstrates that the mass flow does take place directly through the solid sample and the barrier is effective in blocking the flow.

The 95% porosity aerogel disk in *C-A* was cut to be 10% thicker than the width of the sample space. Upon compression, the sample space is completely filled with aerogel. The melting boundary of solid ^{4}He grown in aerogel is found in this and another experiment [20] to be elevated to nearly 27.3 bars from the bulk melting pressure at 25.3 bars. Once the growth of the solid in aerogel is completed, i.e., the liquid in the liquid-solid coexistence region is replaced completely with the solid, a pressure difference across the sandwich (e.g., with *PL* at 28.5 bars and *PR* at 27.3 bars) is found to persist for the duration of observation (more than 56 h) provided the temperature of the solid is kept below 0.8 K. This indicates a complete absence of flow across the solid. Above 0.8 K, thermal-diffusion-induced mass flow is found [21,22]. A total of five attempts were made and no evidence of mass flow was found in any of these attempts below 0.8 K. More details on the growth of a solid in aerogel and the search for mass flow can be found in Supplemental Material Sec. V [16]. The absence of flow through *C-A* establishes conclusively the causal relation that the dislocation network in solid ^{4}He is responsible for the observed mass flow.

Figure 3 shows the mass flow rate from *C-R*, *C-G*⊥, and *C-G*∥ are comparable and similarly sample dependent. This is the case in spite of the contrasting orientations of the ^{4}He solid crystals in *C-G*∥ and *C-G*⊥. As noted above, there is evidence that the crystal orientation of the *C-G*∥ cell is indeed different from the *C-R* and *C-G*⊥ cells. Specifically, only the *C-G*∥ samples show a flattening of the mass flow rate below 0.1 K. The superclimb of edge dislocations on the basal plane is expected to supplant the mass flow in the *C-G*⊥ cell but not in the *C-G*∥ cell. The similar flow rate found in *C-G*⊥ and *C-G*∥ means the superclimb of edge dislocation along the basal plane is not an important factor in determining the mass flow rate. It appears the superclimbing model as proposed [8,9] may require modifications in order to correctly account for the mechanism in densifying the solid during the transport of ^{4}He atoms through the dislocation network. For example, there are theoretical models that indicate a helical shape screw dislocation can also exhibit superclimb that supplants mass flow [9].

Since Vycor and AGC40 porous glasses have atomically random and porous micro-structures, the first few (interfacial) layers of solid ^{4}He grown on the glass surface are highly disordered and also "glassy" in their atomic structure. In addition to the configuration of the dislocation network within the "bulk" solid, the measured mass flow rate also depends on how the dislocation lines are connected to the superfluid in the porous glass through this glassy interfacial layer. This interfacial region also affects the densification (from superfluid to solid) and de-densification (from solid to superfluid) processes as mass is transported across the liquid-solid and solid-liquid interfaces. Since the exact atomic structure of this glassy layer depends very sensitively on exactly how the solid samples are grown, it cannot be duplicated from sample to sample. The variations in the atomic structure of this interfacial layer and the configuration of the dislocation network are the reasons for the observed sample dependence in the mass flow rate.

Figure 4 shows the highest mass flow rate at 0.1 K found among all the solid samples grown in each of the 8-μm, 2-cm (from UMass), *C-R*, *C-G*⊥, and the *C-G*∥ cells as a function of the thickness of the samples. We have chosen to plot the result from the solid sample that shows the highest observed flow rate because that may correspond to the optimal condition for mass flow through the superfluid-solid-superfluid sandwich and make the comparison among the different sample cells meaningful. Interestingly, this plot show that the flow rate decays logarithmically with the thickness of the solid samples, which should scale with the path length of the dislocation lines. The averaged flow rate shows a similar logarithmic dependence on sample thickness as shown in Fig. S5 in Supplemental Material Sec. VI [16].

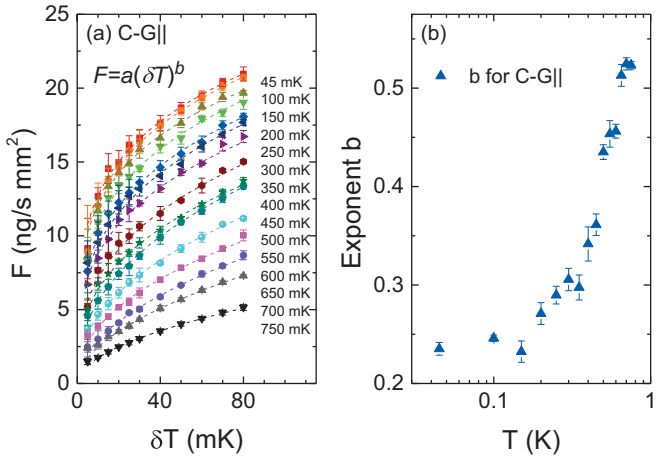

FIG. 5. (a) Mass flow rate of asolid sample of 25.75 bars at different temperatures in the C-$G\|$ cell as a function of δT, the temperature difference of the superfluid reservoirs. δT is proportional to the fountain pressure. The dashed lines show the fit $F = a(\delta T)^b$. (b) Value of the exponent b as a function of solid ^{4}He sample temperature. Exponent b is found to be 0.24 for $T < 150$ mK. and increases rapidly with the sample temperature.

One of the most fascinating aspects of this phenomenon is that once the mass flow has been initiated by a pressure difference (ΔP) across the superfluid-solid-superfluid sandwich by either direct injection of ^{4}He or by the fountain effect, the mass flow rate is not proportional to the diminishing ΔP as in an ordinary fluid; instead, it remains a constant value and ends abruptly when $\Delta P = 0$ [5,6]. This behavior is particularly obvious at low temperatures [6]. This suggests the flow is characterized by a well-defined "flowing mass fraction" with a fixed flow velocity, similar to that found in a superfluid system with a superfluid fraction and superfluid velocity. In this respect the mass flow through the solid is superfluidlike. On the other hand, since the dislocation lines with superfluid cores are one-dimensional objects, it is natural to examine the mass flow phenomenon as a bosonic Luttinger liquid system. Figure 5(a) shows the mass flow rate of the solid samples in C-$G\|$ at different temperatures as a function of δT, the temperature difference of the two bulk liquid reservoirs. δT is proportional to the fountain pressure. The mass flow rate is found to increase sublinearly with fountain pressure. This is analogous to the dependence of current on voltage in a fermionic Luttinger liquid system [23,24]. The dashed lines are fits of the data of the form $F = a(\delta T)^b$. Figure 5(b) shows the value of b as a function of the sample temperature. The value of b is found to be 0.24 for a solid sample below 150 mK and increases rapidly with T for $T > 150$ mK. The increase in the value of b at higher temperatures may be the result of the onset of thermal dissipation in the dislocation network. Similar behaviors are found for two other samples in the C-$G\|$ cell, three samples in C-R, and also one sample in the 8-μm cell. Results on some of these samples are shown in Supplemental Material Sec. VII [16]. The exponent b found in the 2-cm-thick solid samples is 0.32, in reasonable agreement with the result reported here. However, the exponent value for the 2-cm samples shows no noticeable temperature dependence between 0.1 and 0.5 K [3,5]. We note that the value b in a nanotube and edge state in the quantum Hall, two-fermionic systems, are found respectively to be 0.33–0.38 [25] and 2.7 [26].

To conclude, our measurements with sample cells with a barrier and solid ^{4}He grown in aerogel conclusively showed that a dislocation network in the solid is responsible for mass flow through superfluid-solid-superfluid sandwiches. We found the mass flow rate in C-$G\|$ and C-$G\perp$ with solid ^{4}He crystals with contrasting orientations to be comparable and similarly sample dependent. This similarity suggests the superclimb of the edge dislocation is not a dominant parameter in determining the mass flow rate. It appears the exact configuration of the dislocation network in solid ^{4}He samples and how the dislocation lines are connected through an interfacial glassy solid layer to the superfluid in the porous glass are very sensitive to how the solid samples are initially grown. This sensitivity is likely the reason for the sample-dependent mass flow rate found in the different sample cells. We found that the mass flow rate decays logarithmically with the thickness of the solid samples and decays exponentially with the sample pressure. It is interesting that the mass flow displays both superfluidlike and Luttinger liquid characteristics.

We acknowledge informative discussions with Anatoly Kuklov, Robert B. Hallock, and Luciano Reatto. This research is supported by NSF under Grant No. DMR-1707340.

[1] M. W. Ray and R. B. Hallock, Phys. Rev. Lett. **100**, 235301 (2008).
[2] M. W. Ray and R. B. Hallock, Phys. Rev. Lett. **105**, 145301 (2010).
[3] Y. Vekhov and R. B. Hallock, Phys. Rev. Lett. **109**, 045303 (2012).
[4] Y. Vekhov, W. J. Mullin, and R. B. Hallock, Phys. Rev. Lett. **113**, 035302 (2014).
[5] Y. Vekhov and R. B. Hallock, Phys. Rev. B **92**, 104509 (2015).
[6] J. Shin, D. Y. Kim, A. Haziot, and M. H. W. Chan, Phys. Rev. Lett. **118**, 235301 (2017).
[7] M. Boninsegni, A. B. Kuklov, L. Pollet, N. V. Prokof'ev, B. V. Svistunov, and M. Troyer, Phys. Rev. Lett. **99**, 035301 (2007).
[8] S. G. Söyler, A. B. Kuklov, L. Pollet, N. V. Prokof'ev, and B. V. Svistunov, Phys. Rev. Lett. **103**, 175301 (2009).
[9] A. B. Kuklov, Phys. Rev. B **92**, 134504 (2015).
[10] Z. G. Cheng and J. Beamish, Phys. Rev. Lett. **117**, 025301 (2016).
[11] A. C. Pierre and G. M. Pajonk, Chem. Rev. **102**, 4243 (2002).
[12] N. Mulders, J. T. West, M. H. W. Chan, C. N. Kodituwakku, C. A. Burns, and L. B. Lurio, Phys. Rev. Lett. **101**, 165303 (2008).

[13] A. Haziot, A. D. Fefferman, J. R. Beamish, and S. Balibar, Phys. Rev. B **87**, 060509(R) (2013).
[14] F. Souris, A. D. Fefferman, H. J. Maris, V. Dauvois, P. Jean-Baptiste, J. R. Beamish, and S. Balibar, Phys. Rev. B **90**, 180103(R) (2014).
[15] S. Ramesh and J. D. Maynard, Phys. Rev. Lett. **49**, 47 (1982).
[16] See Supplemental Material at http://link.aps.org/supplemental/10.1103/PhysRevB.99.140502 for details about the cleaning process of the HOPG substrate, temperature dependence, phase boundary, pressure dependence, aerogel result, logarithmic dependence, and sublinear dependence of the mass flow rate, which includes Refs. [5,6].
[17] Advance Glass and Ceramics, http://porousglass.com.
[18] S. Sasaki, F. Caupin, and S. Balibar, Phys. Rev. Lett. **99**, 205302 (2007).
[19] S. Sasaki, F. Caupin, and S. Balibar, J. Low Temp. Phys. **153**, 43 (2008).
[20] H. Matsuda, A. Ochi, R. Isozaki, S. Minami, R. Nomura, J. Pollanen, W. P. Halperin, and Y. Okuda, Phys. Rev. B **94**, 024509 (2016).
[21] J. Day and J. Beamish, Phys. Rev. Lett. **96**, 105304 (2006).
[22] A. Suhel and J. R. Beamish, Phys. Rev. B **84**, 094512 (2011).
[23] F. D. M. Haldane, J. Phys. C **14**, 2585 (1981).
[24] C. L. Kane and M. P. A. Fisher, Phys. Rev. Lett. **68**, 1220 (1992).
[25] M. Bockrath, D. H. Cobden, J. Lu, A. G. Rinzler, R. E. Smalley, L. Balents, and P. L. McEuen, Nature (London) **397**, 598 (1999).
[26] A. M. Chang, L. N. Pfeiffer, and K. W. West, Phys. Rev. Lett. **77**, 2538 (1996).